scientific reports

Check for updates

OPEN

Superior replication, pathogenicity, and immune evasion of a Texas dairy cattle H5N1 virus compared to a historical avian isolate

Cassio Pontes Octaviani[1,6]✉, Pinghan Huang[1,6]✉, Peng Bi-Hung[2], Gregory C. Gray[1,3,4] & Chien-Te K. Tseng[1,5]✉

The current outbreak of highly pathogenic avian influenza (HPAI) viruses of the H5N1 subtype clade 2.3.4.4b in dairy cattle in the United States has affected nearly 900 dairy farms and resulted in at least 39 human infections, putting health authorities and the scientific community on high alert. Here we characterize the virus growth properties and host-pathogen interactions of an isolate obtained from a sick dairy cow in Texas in vitro and in vivo and compare it to an older HPAI isolate. Despite so far being associated with mild disease in human patients, the cattle H5N1 virus showed superior growth capability and rapid replication kinetics in a panel of human lung cell lines in vitro. In vivo, cattle H5N1 exhibited more intense pathogenicity in mice, with rapid lung pathology and high virus titers in the brain, accompanied by high mortality after challenge via different inoculation routes. Additionally, the cattle H5N1 demonstrated efficient antagonism of overexpressed RIG-I- and MDA5-mediated innate antiviral signaling pathways. In summary, this study demonstrates the profound pathogenicity and suggests a potential innate immune escape mechanism of the H5N1 virus isolated from a dairy cow in Texas.

Since 1997, highly pathogenic avian influenza (HPAI) A viruses of the A/goose/Guangdong/1/1996 (H5N1) lineage have often been the cause of devastating outbreaks in domestic and wild bird flocks, occasionally crossing the species barrier to infect mammals, including humans, and raising a concern that such viruses may eventually become more pathogenic and/or transmissible in humans[1]. This concern has grown over the last few years, with frequent reports of outbreaks of clade 2.3.4.4b viruses in domestic and wild birds, infections in mammals in several countries and continents, and even more alarmingly, infections of large groups of wild and farmed mammals such as seals and minks, with evidence of possible mammal-to-mammal transmission[2–4].

A whole new chapter in the history of HPAI started in March 2024, when an outbreak in dairy cows in the state of Texas was first reported. Affected cows presented with decreased feed intake, decreased rumination time, mild respiratory signs, lethargy, signs of dehydration, and abrupt drop in milk production with altered milk characteristics (i.e., a thickened, yellow appearance). Lethality is low, and most cows recover in a few weeks, although milk production may remain low for longer periods. Strikingly, infection is characterized by high tropism of the HPAI virus for the mammary gland tissue, resulting in a viral mastitis and substantial viral shedding in the affected milk[5,6]. This current outbreak is highly unusual, as until now, cattle were generally seen as only infrequently infected by influenza viruses, most commonly influenza D. Though it has long been known that the bovine mammary glands are susceptible to experimental infection by influenza viruses upon intramammary inoculation[7], spontaneous mammary infections with any influenza viruses had never been reported. Importantly, many farms reported concurrent deaths of domestic and peridomestic animals, most notably birds (grackles, pigeons) and outdoor domestic cats which are believed to have acquired infection likely through the consumption of contaminated raw milk from the sick cows[8].

[1]Department of Microbiology and Immunology, University of Texas Medical Branch, Galveston, TX, USA. [2]Department of Neurobiology, University of Texas Medical Branch, Galveston, TX, USA. [3]Department of Internal Medicine (Division of Infectious Disease), University of Texas Medical Branch, Galveston, TX, USA. [4]Department of Global Health, University of Texas Medical Branch, Galveston, TX, USA. [5]Centers for Biodefense and Emerging Diseases, University of Texas Medical Branch, Galveston, TX, USA. [6]Cassio Pontes Octaviani and Pinghan Huang: These authors contributed equally to this work. ✉email: caoctavi@utmb.edu; pihuang@utmb.edu; sktseng@utmb.edu

Although the first documented cases were reported in March, epidemiological information and phylogenetic analyses indicate the dairy cattle HPAI outbreak may have started several months earlier, in late 2023[9]. Since then, it has quickly spread through the United States and, as of December 16, 2024, has reached 16 states, being confirmed in 853 dairy herds[10], making it by far the most extensive and prolonged instance of mammal-to-mammal transmission of HPAI viruses known to date. As of December 26, 2024, CDC has confirmed 65 human H5 influenza infections in the United States, of which 39 were associated with infected dairy cows and 23 with exposure to infected poultry[11], most of which have been benign. The continuous circulation of HPAI A(H5N1) in cattle is a major concern. It creates an ideal condition for adaptation of the virus to further increase the transmissibility among the mammalian hosts. Moreover, the proximity of cows and people also favors reassortment with human influenza viruses. Adaptation and reassortment are the two major mechanisms for the generation of pandemic influenza[12].

To better understand this threat, an understanding of the growth properties and the host-pathogens interactions of the cattle HPAI A(H5N1) is paramount. In this study, we characterized the growth properties of HPAI A(H5N1) isolate A/cattle/Texas/56283/2024(H5N1) (cattle-HPAI) in vitro, and its pathogenicity, tissue tropism and infection kinetics in vivo, while comparing it with an older HPAI isolate, A/whooper swan/Mongolia/244/2005(H5N1) (M244/05)—a classical avian isolate that is known to be pathogenic in mammalian animals including mice, ferrets and non-human primates[13–16]. Finally, we identified a potential mechanism by which cattle H5N1 isolate antagonizes the host innate immune response.

Results

Cattle-HPAI has superior growth capability to M244/05 in human lung cell lines

To shed light into the host-pathogen interactions of cattle-HPAI in mammalian cells and the potential implications for human health, we investigated the in vitro growth properties of the virus in a panel of cell lines consisting of human lung epithelial (A594, Calu-3) and fibroblastic (MRC5), as well as canine and bovine kidney epithelial (MDCK and MDBK, respectively) cell lines, in parallel with M244/05. Our results show that cattle-HPAI has substantially faster and higher growth properties in most cell lines tested, compared to M244/05 (Fig. 1). Curiously, the only exception was the bovine cell line MDBK, where although cattle-HPAI did grow slightly better, the difference was not statistically significant. Importantly, cattle-HPAI showed strongly enhanced growth capability in all human respiratory cell lines tested, reaching approximately one hundred-fold higher titers than M244/05 at 48 h post-infection in each of them.

We next assessed the pathogenicity of the bovine isolate in the mouse model. To that, groups of 8-week-old BALB/c mice were anesthetized with isoflurane and intranasally inoculated with different doses of cattle-HPAI, after which they were monitored daily for morbidity (clinical signs, body weight loss) and mortality. Cattle-

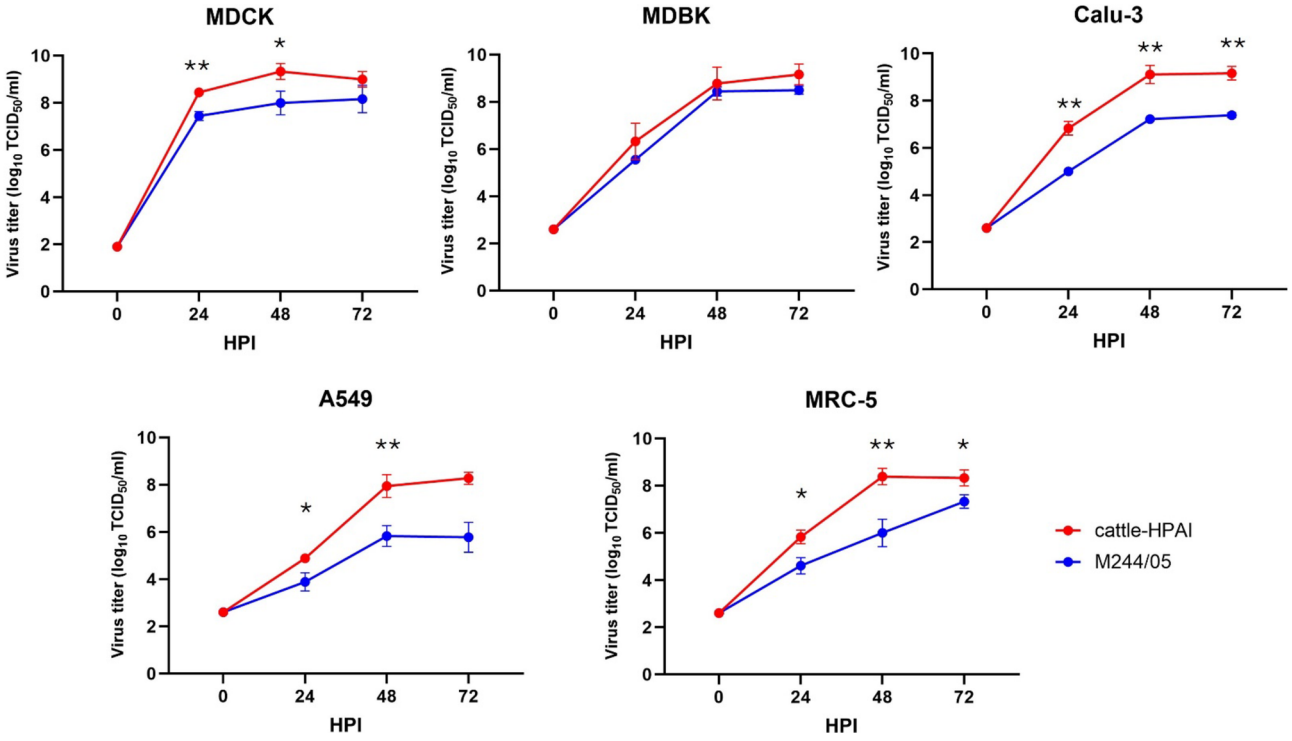

Fig. 1. Comparative growth kinetics of cattle-HPAI and M244/05 in mammalian cell lines in vitro. Cells were infected at a multiplicity of infection of 0.0002 (MDCK) or 0.001 (MDBK, Calu-3, A594 and MRC-5). Virus yields at the indicated time points were determined by $TCID_{50}$ assay in MDCK cells. Data represent the means of three independent infections ± standard deviation. HPI: hours post-infection. * $p < 0.05$, ** $p < 0.01$.

HPAI proved to be highly pathogenic in this mouse model, showing a median lethal dose (MLD_{50}) of only 2.5 $TCID_{50}$. In addition, the disease progression showed to be extremely fast, with most mortality happening on day 4 post-infection, even after challenge with low virus doses (Fig. 2). This contrasts with the disease progression caused by M244/05, which showed an MLD_{50} of 147 $TCID_{50}$, with mortality occurring eight to nine days after intranasal challenge with 10^3 $TCID_{50}$ of virus (Supplementary Fig. S1).

Considering epidemiological information of dead peridomestic animals on dairy farms affected by the bovine H5N1 outbreak, presumably from the consumption of raw milk[8], and the important implications for human health of this potential infection route, we investigated the pathogenicity of cattle-HPAI in mice through the digestive route. After anesthesia with isoflurane, we inoculated groups of BALB/c mice through oral gavage with 100 µl of grade A raw cow milk obtained from a local dairy farm, spiked with MDCK-grown cattle-HPAI to a challenge dose of 10^3 or 10^6 $TCID_{50}$ of virus. Cattle-HPAI caused disease and death in 80% of mice orally inoculated with either virus challenge dose, thus confirming that it is indeed infective and highly pathogenic also through the digestive route. (Supplementary Fig. S2). However, in addition to the lower lethality observed after oral challenge, the infection dynamics were different from the respiratory route, with mortality spread over a longer period, from 3 to 7 days post-infection (DPI), as opposed to 4 to 6 DPI in the case of intranasal challenge. This result is consistent with previous reports[17,18].

To further expand our study of the pathogenicity of cattle-HPAI in mice, we intranasally inoculated groups of 16-week-old C57BL/6 mice with 10 or 100 $TCID_{50}$ of cattle-HPAI, then monitored them daily for body weight loss and mortality. We observed similar outcomes to the BALB/c model, with infection leading to death in all mice challenged with 100 $TCID_{50}$, and 4 out of 5 mice in the group challenged with 10 $TCID_{50}$. Besides the slightly lower lethality rate compared to BALB/c, the course of infection in these older C57BL/s mice was also less sharp, characterized by relatively lower body weight loss and more protracted time to death (Supplementary Fig. S3).

Cattle-HPAI exhibits faster replication kinetics than M244/05 in the lungs and brains of BALB/c mice

We next assessed the histopathology and virus tissue tropism of cattle-HPAI, with a focus on lung and brain. To that, we intranasally inoculated six mice with 10 $TCID_{50}$ of cattle-HPAI, a dose equivalent to 4 MLD_{50}. At 2 and 4 DPI, three mice were euthanized, their lungs and brains harvested and subjected to homogenization and virus titration (Fig. 3a), as well as formalin fixation and hematoxylin and eosin (H&E) staining (Fig. 4a, d), and immunohistochemistry (IHC) (Figs. 5c and 6a). For comparison, we also inoculated 12 mice with 750 $TCID_{50}$ of M244/05, a dose equivalent to 5 MLD_{50} (Supplementary Fig. S1), and assessed tissue tropism of the virus (Fig. 3b) and histopathology (Figs. 4b, c and e, 5d and 6b) at 2, 4, 6 and 8 DPI. We deliberately chose to use a higher challenge dose for the latter virus, aiming at adjusting for the known differences in disease dynamics observed in terms of morbidity and mortality between the two viruses (Fig. 2, Supplementary Fig. S3), so that a better comparison could be made. Cattle-HPAI reached an average titer in the lungs of mice of 10^6 $TCID_{50}$ per gram of tissue after only two days, and 10^8 $TCID_{50}$/g of tissue at 4 DPI, a time point by which all three mice were either moribund or found dead. Moreover, cattle-HPAI also reached the brain of mice strikingly fast, being detected in the brains of two out of three mice at 2 DPI and reaching a high titer of about 10^7 $TCID_{50}$/g in the brains of all three mice at 4 DPI (Fig. 3a). M244/05 also showed a similar titer of about 10^6 $TCID_{50}$/g in the lungs of mice at 2 DPI, progressing to 10^7 $TCID_{50}$/g at 4 DPI, and declining slightly though remaining relatively high in the lungs through 8 DPI. However, in stark contrast to cattle-HPAI, M244/05 virus was not present in the brains of any mice on day 2; was barely detectable in only one out of three mice on day 4, growing to titers of no more than 10^3 $TCID_{50}$/g of brain tissue by day 8 post-infection (Fig. 3b).

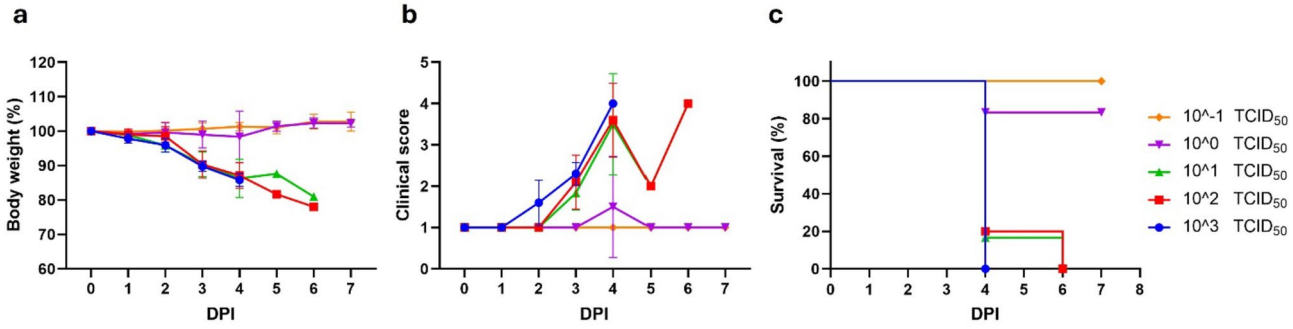

Fig. 2. Morbidity and mortality of BALB/c mice following intranasal challenge with cattle-HPAI. Mice were challenged with doses ranging from 10^{-1} to 10^3 $TCID_{50}$ of virus ($n = 5$ animals per challenge dose), after which they were monitored at least daily for signs of morbidity and mortality. (**a**) Body weight changes. (**b**) Clinical signs were scored. (**c**) Probability of survival. Data points in **a** and **b** represent mean values. Error bars represent standard deviation.

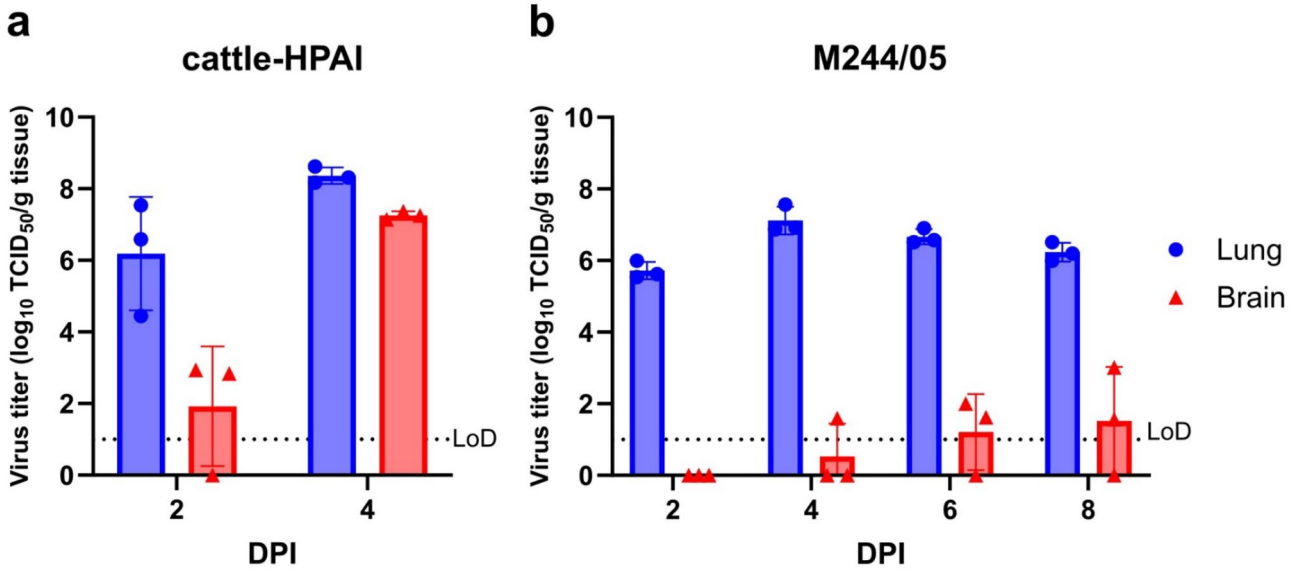

Fig. 3. Lung and brain tissue tropism following IN challenge with cattle-HPAI or M244/05. Mice were intranasally inoculated with 10 $TCID_{50}$ of cattle-HPAI (**A**) or 750 $TCID_{50}$ of M244/05 (**B**) ($n = 6$ for cattle-HPAI, 12 for M244/05). At indicated times post-infection, three mice per group were euthanized, organs were harvested, lysed and subjected to virus titration. Virus titers in lungs and brains at each time point are indicated (mean values ± standard deviation). DPI: days post-infection. Difference in virus yields in lungs of mice infected with cattle-HPAI and M244/05 at 4 DPI (means 8.37 and 7.12 log_{10}, respectively) statistically significant ($p < 0.01$).

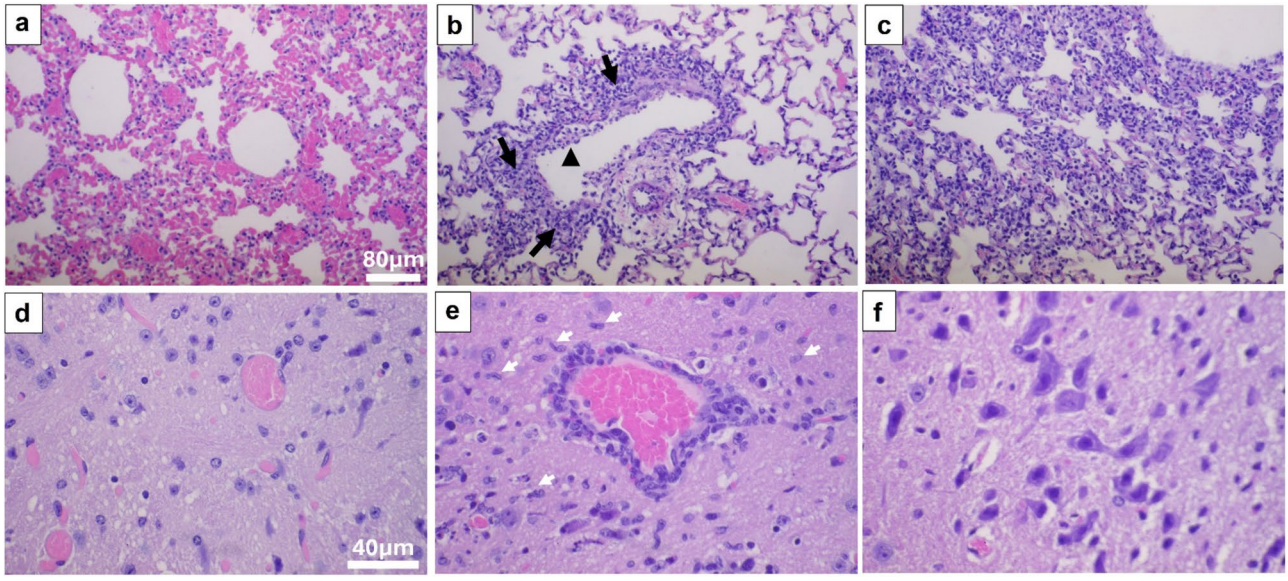

Fig. 4. Histopathology of mouse lung and brain tissue following IN challenge with virus. Lungs (**a**-**c**) and brains (**d**-**e**) were collected from mice challenged with cattle-HPAI (**a** & **d**) or M244/05 (**b**, **c** & **e**). **f**: brainstem area of an uninfected mouse is served for comparison with **d** and **e**. Severe congestion in all vessels in lung (**a**) and brain (**b**) sections of mice challenged with cattle-HPAI at 4 DPI. Few foci of pulmonary edema with fluid in the alveolar space was observed indicating of vascular leakage. Respiratory epithelial cell death (arrowhead) and inflammatory infiltrations (arrows) with lymphocytes and monocytes/macrophages (mononuclear cells) were seen in the lung of mice challenged with M244/05 at 4DPI (**b**) and infiltrations gradually extended from peri-vascular and peri-bronchial/bronchiolar to the alveolar septa at 8DPI (**c**). In the brain of M244/05-infected mice, perivascular cuffing with mononuclear cells and microglial activation (white arrows) were found only in the brainstem at 8 DPI (**e**). A similar brainstem area (**f**) from an uninfected mouse is served for comparison with **d** & **e**. Bar = 80 µm for **a**–**c**, 40 µm for **d**–**f**.

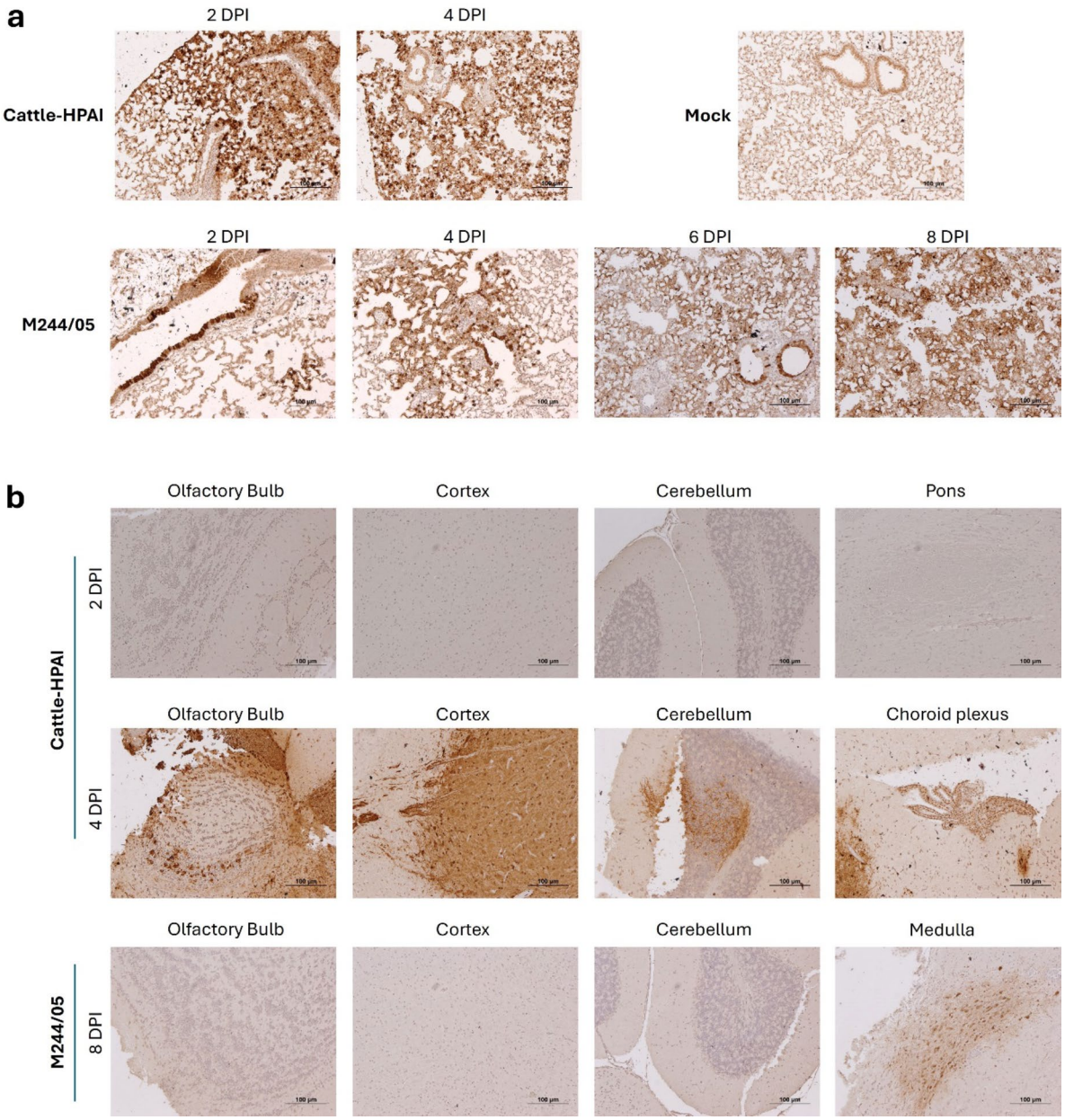

Fig. 5. Detection of virus antigens in lungs of challenged mice. Mice were challenged with 10 $TCID_{50}$ of cattle-HPAI or 750 $TCID_{50}$ of M244/05 and euthanized at the indicated days post-infection. Lungs (**a**) and brains (**b**) were harvested, formalin-fixed and paraffin-embedded, and sections were subjected to immunohistochemistry staining using a mouse anti-influenza M1 antibody. Brown staining indicates presence of influenza virus antigen. In (**a**), lung of a mouse mock-infected with media only is shown for comparison. DPI: days post-infection.

Cattle-HPAI infection causes more severe lung and brain tissue damage than M244/05 in BALB/c mice

Histopathological analysis of tissue samples revealed severe congestion of all blood vessels in lungs (Fig. 4a) of mice challenged with cattle-HPAI at 4 DPI. In addition, few foci of pulmonary edema with fluid in the alveolar space was observed, which is indicative of vascular leakage, but no signs of cell death or inflammatory infiltrations. On the other hand, mice challenged with M244/05 show respiratory epithelial cell death and inflammatory infiltrations with lymphocytes and monocytes/macrophages (mononuclear cells) in the lungs at 4 DPI (Fig. 4b), with infiltrations gradually extending from perivascular and peri-bronchial/bronchiolar to the alveolar septa at 8 DPI (Fig. 4c). Brains of mice challenged with cattle-HPAI showed marked congestion at 4 DPI (Fig. 4d). Mice challenged with M244/05 did not show histopathological signs inflammation in the brain up to 6 DPI; at 8 DPI, perivascular cuffing with mononuclear cells and microglial activation was present in the brainstem only (Fig. 4e), which were absent in the same area of the brain of a mock-infected mouse (Fig. 4f).

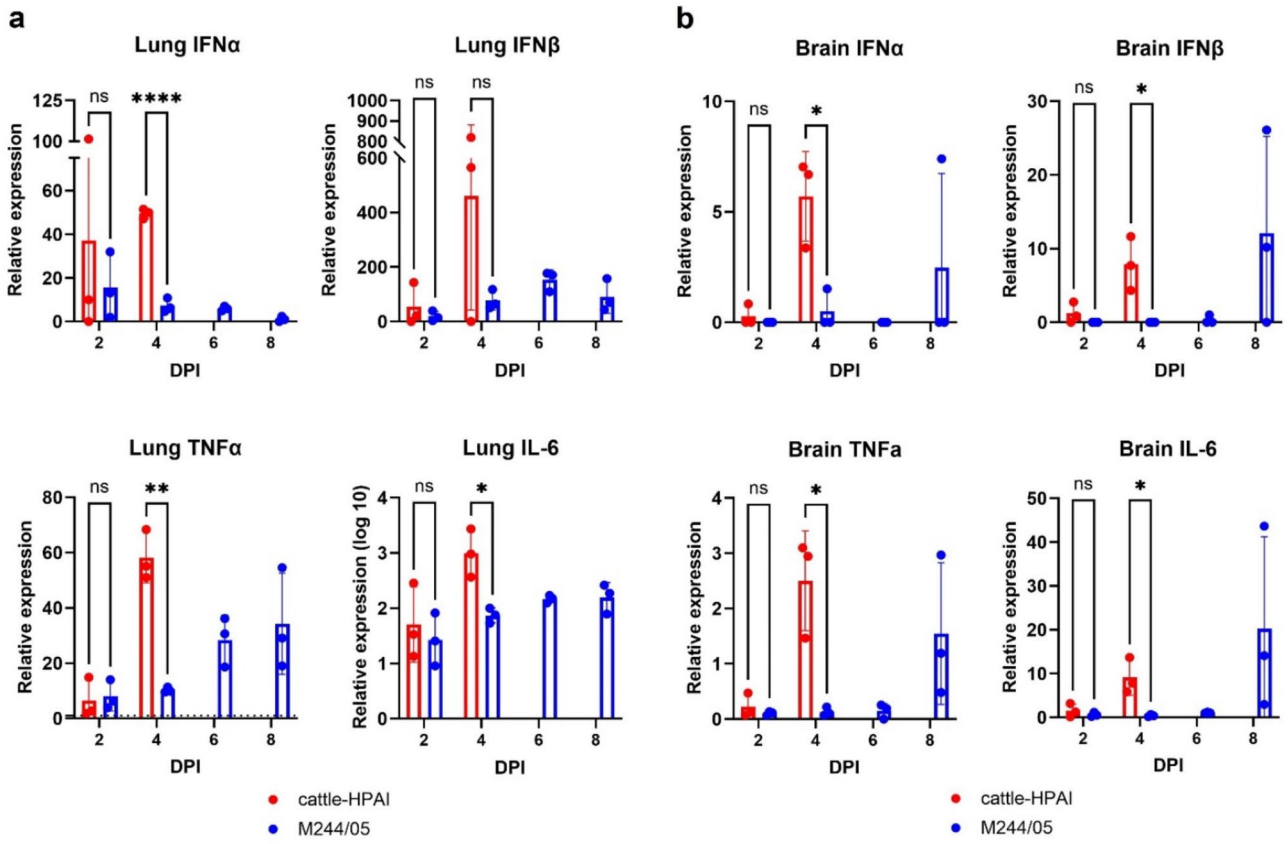

Fig. 6. Expression of cytokines in lungs (**a**) and brains (**b**) of infected mice. Mice were challenged with 10 $TCID_{50}$ of cattle-HPAI ($n=6$) or 750 $TCID_{50}$ of M244/05 ($n=12$). At the indicated times post-infection, three mice per group were euthanized, tissues harvested, lysed and subjected to total RNA extraction for RT-qPCR for quantification of mRNA for the indicated cytokines. Data represent mean values of expression fold change relative to mock, and error bars represent standard variation. * $p<0.05$, ** $p<0.01$, ns: not significant.

To further characterize the tissue tropism of the two viruses, we analyzed tissue sections of mice challenged with cattle-HPAI and M244/05 by IHC staining, using a polyclonal antibody against influenza matrix 1 (M1) protein. Lung of mice challenged with cattle-HPAI showed distinct foci of intense staining in the parenchyma at 2 DPI, and by 4 DPI the whole lung was affected. By contrast, infection in the lungs of mice challenged with M244/05 progressed much more slowly, with discrete foci being detected from 2 DPI to few isolated areas of infection at 4 DPI, eventually affecting most of the lung tissue by 8 DPI (Fig. 5a, Supplementary Fig. S4), which is consistent with the slower growth kinetics in vitro, as well as the slower disease progression in vivo described above. Interestingly, M244/05 associated with particularly strong staining in the bronchiolar epithelium, which was not present in the lungs of mice challenged with cattle-HPAI, whereas both viruses caused staining of the alveolar epithelium.

All mice challenged with cattle-HPAI showed large foci of strong staining affecting different regions of the brain with varying patterns at 4 DPI. Curiously, two of three mice showed intense virus antigen staining in the choroid plexus (Fig. 5b, Supplementary Fig. S5). By contrast, positive staining was only present in the brain of one of three mice challenged with M244/05, with one focus in the brain stem being detected at 8 DPI (Fig. 5b, Supplementary Fig S5). This difference in timing and extent of virus detection in the brain between cattle-HPAI- and M244/05-infected mice is in agreement with the virus titers data (Fig. 3).

We next assessed cytokine expression in the lungs and brains of mice infected with either cattle-HPAI or M244/05 by reverse transcription quantitative polymerase chain reaction (RT-qPCR). Cytokines play a major role in influenza pathogenesis. While in most cases they function to promote an antiviral state in the organism to control infection[19], their overabundance or imbalance can indeed become a pathogenicity factor through the induction of an imbalanced response that increases pathogenicity, in the so-called "cytokine storm", which is a hallmark of HPAI and other highly pathogenic viruses[20–23]. All tested cytokines, i.e., antiviral cytokines type I interferons (IFNα, IFNβ) and proinflammatory cytokines TNFα and IL6, were upregulated at transcriptional level at 4 DPI in mice infected with cattle-HPAI, both in lung and brain tissue. In mice challenged with M244/05, cytokine gene upregulation was reduced or delayed, compared to cattle-HPAI, both in lungs and brains, most of them peaking at 8 DPI (Fig. 6). This is consistent with the disease progression and replication kinetics of these two viruses (Fig. 2, Supplementary Fig. S1).

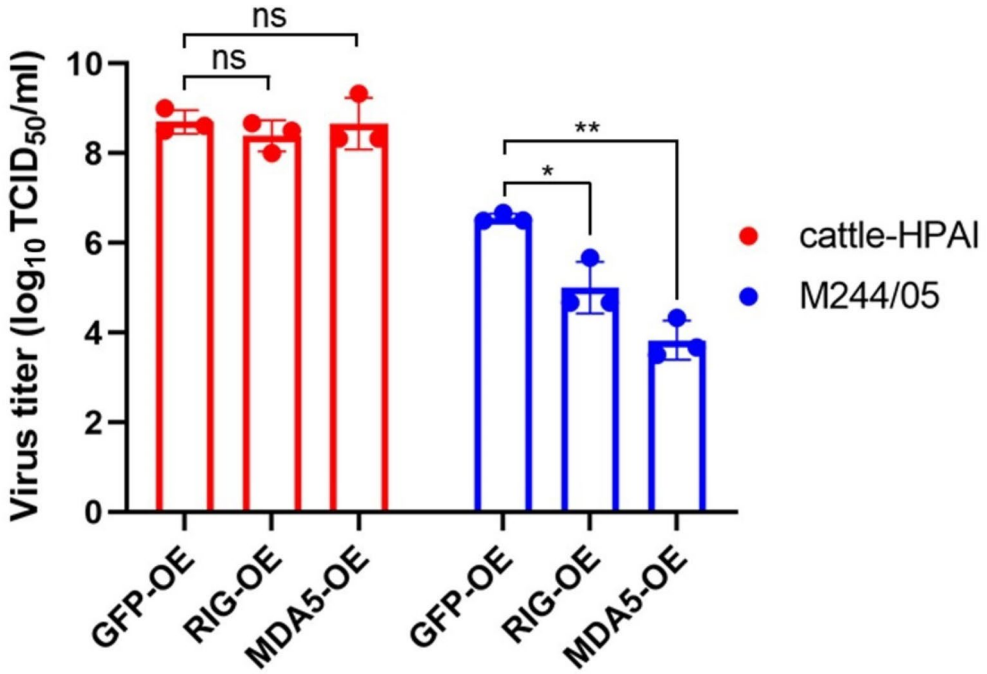

Fig. 7. The effect of RIG-I and MDA5 overexpression on virus growth. Green fluorescent protein (GFP), RIG-I and MDA5 were overexpressed in Calu-3 cells (GFP was included to serve as a negative control) by means of lentiviral transduction and antibiotic selection. Cells were infected at a multiplicity of infection of 0.001 with Cattle-HPAI or M244/05, and incubated at 37 °C for 48 h, when supernatants were harvested and subjected to virus titration. Data represent the mean virus titers in supernatants from three independent infections, and error bars represent standard deviation. * $p < 0.05$, ** $p < 0.01$.

Cattle-HPAI evades RIG-I- and MDA5-mediated interferon immune response

Cattle-HPAI showed greatly enhanced growth capability in vitro and in vivo, along with high pathogenicity associated with fast neurotropism in mice. With this in mind, we set out to explore possible mechanisms for such enhanced growth and pathogenicity. One known such mechanism is the evasion of the innate host immune response by influenza viruses. For example, interferon response is known to be targeted by several influenza proteins, most notably NS1[24], but also PB2, PB1-F2 and HA[25–27]. Innate immune response against viral infections starts with the recognition of viral invasion by pattern-recognition receptors (PRRs), such as retinoic acid-inducible gene I (RIG-I) and melanoma differentiation-associated gene 5 (MDA5), leading to the activation of signaling pathways to induce type I interferons and other proinflammatory cytokines[28,29]. Interferons then promote an antiviral state, blocking virus replication at many levels through the upregulation of interferon-stimulated genes (ISGs)[30,31].

To investigate an evasion of the cellular innate immune response as a possible mechanism for enhanced growth and pathogenicity of cattle-HPAI, we assessed the growth kinetics of the virus in Calu-3 human lung epithelial cells overexpressing RIG-I and MDA5. Here too, we used M244/05 for comparison.

Our results show that while overexpression of RIG-I or MDA5 strongly reduces the yields of M244/05 by 1.5 and 2.7 $\log_{10}$ respectively, they have no effect on the yields of cattle-HPAI (Fig. 7). This indicates that these pathways of innate antiviral response, while effective against M244/05, are ineffectual against cattle-HPAI, suggesting a signaling antagonism by the latter virus.

Discussion

The current global multispecies panzootic caused by HPAI clade 2.3.4.4b H5N1 viruses, which has spread to dairy cattle causing a nationwide outbreak in the United States, has the scientific community and public health authorities on high alert. Accordingly, many measures have been instituted to monitor, contain and stop HPAI A(H5N1) transmission, with seemingly little effect[4]. These interventions have included increased virus surveillance in dairy herds, animal workers, and dairy products, tracking and limiting movement of lactating cows, stepping up biosecurity measures in dairy operations, and recently, mandatory pooled milk screening[32].

Here we report results of our ongoing work for characterizing the host-pathogen interactions of the cattle HPAI A(H5N1) with mammalian hosts in vitro and in vivo.

Other groups have studied dairy cattle H5N1isolates in mouse models and compared its pathogenicity with other 2.3.4.4b clade viruses, as well as other more distant HPAI strains (e.g. A/Vietnam/1203/2004) and even human H1N1 viruses[17,18]. Here we expand this comparative characterization by pairing the cattle-HPAI with yet another classical H5N1 isolate, M244/05. We chose this classical and well-characterized yet phylogenetically distinct strain of HPAI considering its relevance in the context of viral evolution, zoonotic potential and public

health concern. Choosing a pure-avian strain to compare with cattle-HPAI provides an opportunity to study the basis of viral adaptation to cattle and other mammalian species, which could provide new insights into the risk of human infection and potential spread.

We show that the cattle HPAI A(H5N1) is highly lethal to mice, with an MLD_{50} of only 2.5 $TCID_{50}$ upon intranasal challenge of BALB/c mice, and that even very low infectious doses can kill mice in only 4 days. Cattle-HPAI virus had faster replication kinetics especially in the brains of challenged mice, compared with M244/05—after challenging mice with 10 $TCID_{50}$ of cattle-HPAI or 750 $TCID_{50}$ of M244/05, the growth of the former overtook that of the latter by 2 DPI in the brains and 4 DPI in the lungs. In our hands, M244/05 showed limited replication in the brain, with virus being detected at low levels in only one of 3 animals at 4DPI, progressing to 2 out of 3 mice at 6 and 8 DPI, with maximum titers of 10^2 and 10^3 $TCID_{50}$/g respectively. This finding is consistent with a previous report[14]. However, another report saw more robust virus growth of M244/05 in the brain of mice, with virus being detected in all animals and reaching mean titers of 10^4 egg-infective doses (EID) at 9 DPI[13].

We also show that the high pathogenicity of cattle-HPAI in mice is not strain- or age-specific, as challenge of older C57BL/6 mice led to similar outcome.

Upon histopathological analysis, lungs of cattle-HPAI-infected mice showed severe congestion and edema accompanied by vascular leakage, in the absence of inflammatory infiltration at 4 DPI, whereas lungs of M244/05-infected mice showed marked cell death and perivascular inflammatory infiltration, despite cattle-HPAI showing more extensive virus antigen staining at this time post-infection. This can be interpreted as a sign of early, overwhelming immunosuppression caused by the cattle isolate. Mice challenged with cattle-HPAI also showed intense congestion in the brain, which was not observed with M244/05, which is in keeping with the detection of virus antigens by IHC and the virus titers data in that organ.

Eisfeld et al. characterized the pathogenicity of a New Mexico isolate of HPAI A(H5N1), A/dairy cattle/New Mexico/A240920343-93/2024, in vivo using the same mouse model we report here. That isolate showed an MLD_{50} of 31.6 PFU —a lethal dose over one log higher than the Texas isolate used in the current study. Moreover, the Texas isolate characterized here showed much faster disease progression, with most mortality occurring at 4 DPI even at the lowest infectious doses, and with no mouse surviving past day 4 after challenge with 10^3 $TCID_{50}$ of virus, while similar challenge with the New Mexico strain would take twice as long (eight days) to kill all mice. In another study by the same group, it was found that two other strains of cattle H5N1, one isolated from a cow and another from a human patient, both in Texas, were both highly lethal at very low challenge doses such as 10 and even 1 PFU[33], which is consistent with our findings.

The Texas isolate used in our study also showed faster replication kinetics in the brain: after challenge with only 10 $TCID_{50}$, virus was detected in the brains of 2 out of 3 mice already at 2 DPI, with titers to the order of 10^3 $TCID_{50}$/g of tissue, and 3 out of 3 mice at 4 DPI, all of them with titers above 10^7 $TCID_{50}$/g of brain tissue. By contrast, as reported by Eisfield et al., 2024, after intranasal challenge of mice with 100 PFU of the New Mexico strain, no mice showed virus detection in the brain by 4 DPI; only half of the mice showed detectable virus in the brain at 7 DPI, while in another experiment, after challenge with 10^3 PFU, virus was first detected in the brains of mice only at 6 DPI, in 4 out of 5 mice, with a mean titer of around 10^4 PFU/g. Taken together, these results indicate that there is substantial variation in the pathogenicity among different isolates of the HPAI A(H5N1) currently circulating in dairy cattle in the United States. Further efforts should focus on determining the molecular determinants for the differences observed in pathogenicity and neurotropism among the different cattle H5N1 isolates, and the possible mechanisms for such.

One of the distinguishing characteristics of the current HPAI outbreak in dairy cattle is the fact that the mammary gland is the primary organ affected, leading to the production of infected milk containing high titers of infectious viruses, which may pose a severe risk to people through the consumption of raw milk, which is emphasized by the occurrence of dead peridomestic animals on dairy farms affected, attributable to the consumption of raw milk. With that in mind, we explored the pathogenicity o cattle-HPAI in mice through the oral route. Eisfeld et al. (2024) reported a similar experiment; however, they administered the inocula by pipetting to the back of the throat. Considering that the oropharynx is also part of the upper respiratory system, direct respiratory infection by such methodology cannot be ruled out, a fact further stressed by the report that, after inoculation, mice showed milk in the nasal cavity[34]. Therefore, we chose to inoculate the mice through oral gavage, to ensure challenge through the digestive system while preventing the possibility of direct respiratory infection. Cattle-HPAI retained its high pathogenicity also after oral challenge, which is consistent with previous reports[17,18]. Although we did not perform challenge of mice with M244/05 through oral gavage, it has been reported that that virus is also capable of infecting mice through that route[14].

We also directed efforts towards the characterization of the interactions of the cattle H5N1 virus with mammalian host cells in vitro. We found that cattle-HPAI has extremely high virus fitness in at least three human lung cell lines —A594, Calu-3 and MRC-5—growing to two log_{10} higher titers at 48 HPI than M244/05. This is consistent with a report from Gu et al., 2024, who found that a cattle-derived H5N1 isolated from a human patient in Texas grew faster than A/Vietnam/1203/2004 in human primary lung alveolar cells, reaching very high titers. This finding may have important implications for human health: even though all reported cases of H5N1 infections in humans acquired from exposure to cattle have been mild, severe outcomes in case of lung infection by the virus might seem likely in the unpredictable future. This is further emphasized by recent cases of severe human H5N1 infection in Canada and the United States by viruses of the clade 2.3.4.4b, associated with the ongoing poultry outbreak of HPAI[35,36].

Using human lung Calu-3 cells overexpressing either RIG-I or MDA5, we also found that the growth capacity of cattle H5N1 virus is unabated, in contrast to that of M244/05 virus, suggesting a more efficient interferon antagonism may account at least in part for its superior growth kinetics and, possibly, pathogenicity. Interestingly, despite the resistance to interferon signaling observed in vitro, we did see an induction of type I interferons at the

transcription level in both lungs and brains of mice infected with cattle-HPAI, in keeping with the upregulation of the pro-inflammatory cytokines tested, as is typical of a cytokine storm associated with highly pathogenic virus infection. A similar scenario has been observed with other highly pathogenic viruses – for instance, while Ebola is known to antagonize the interferon system by a variety of mechanisms[37–40], highly elevated expression of interferons is nevertheless a hallmark of Ebola infection[41–43]. It is conceivable that an inhibition of antiviral signaling may confer an advantage to virus replication at an early stage leading to overwhelming infection, before an exuberant inflammatory response at cytokine level takes over, leading to the indiscriminate overstimulation of inflammatory pathways (cytokine storm scenario). Further efforts towards the elucidation of the molecular mechanisms involved in this innate immune antagonism are warranted.

Methods

Biosafety and ethics statement

All work with live viruses was conducted under Biosafety Level 3-Enhanced at the Galveston National Laboratory. Sample inactivation followed protocols approved by the University of Texas Medical Branch (UTMB) Institutional Biosafety Committee (IBC). All animal experiments and procedures were approved by the Institutional Care and Use Committee (IACUC) of the UTMB. We confirmed that all experiments in this study were performed in accordance with the relevant guidelines and regulations. All the procedure of the study is followed by the ARRIVE guidelines.

Cells

Madin-Darby canine kidney (MDCK), Madin-Darby bovine kidney (MDBK), human lung carcinoma epithelial A549, and human lung fibroblast MRC-5 cells were cultured in Minimal Essential Medium (MEM) supplemented with 10% fetal bovine serum (FBS), 4 mM L-glutamine, 100 U/mL penicillin-streptomycin, and 0.25 µg/mL Amphotericin B. Human lung adenocarcinoma epithelial Calu-3 cells were cultured in MEM supplemented with 20% FBS, 4 mM L-glutamine, 100 U/mL penicillin-streptomycin, and 0.25 µg/mL Amphotericin B. Cells were maintained in a humidified incubator at 37 ˚C and 5% CO_2. MDCK and MDBK cells were kindly gifted by Drs. Thomas G. Ksiazek and Junki Maruyama, respectively. Human lung carcinoma epithelial A549, human lung fibroblast MRC-5 and human lung adenocarcinoma epithelial Calu-3 were purchased from American Type Culture Collection (ATCC, Manassas, VA).

Calu-3 cells stably overexpressing retinoic acid-inducible gene I (RIG-I) and melanoma differentiation-associated gene 5 (MDA5) were prepared by lentiviral transduction and antibiotic selection, as previously described[44], with modifications. Briefly, we generated the lentiviral vector by cloning the cDNA of the innate immune molecules, each N-terminally fused to an HA tag, into expression vector pPS-EF1-LCS-T2A-puro (Clone-it™ enzyme-free lentivectors). The expression vector was co-transfected with accessory vectors pPACKH1-GAG, PPACKH1-REV and pVSV-G of the pPACKH1 HIV Lentivector Packaging Kit (System Biosciences) into 293T cells to generate lentiviral vector particles, which were used to transduce Calu-3 cells. After transduction, transduced cells were selected by addition of 5 µg/mL in the medium. Overexpression of transgenes was confirmed by Western blotting (Supplementary Fig. S6).

Viruses

A/cattle/Texas/56283/2024 (H5N1) (GenBank accession numbers PP600140–7) was provided by Gregory C. Gray and is shared via the World Reference Center for Emerging Viruses and Arboviruses (WRCEVA). A/whooper swan/Mongolia/244/2005 (H5N1) (GenBank accession numbers GU186700–7) was also kindly shared with Professor Gray by the US CDC. The viruses were propagated in MDCK cells, in MEM supplemented with 0.3% bovine serum albumin (BSA), MEM vitamins, MEM amino acids, L-glutamine, antibiotics/antimycotic, and 0.5 µg/mL TPCK-treated trypsin, as previously described[45].

In vitro infections

In vitro infections for growth kinetics determination were carried out in 12 well plates. MDCK cells grown to a confluent monolayer were infected at a multiplicity of infection (MOI) of 0.0002 in MEM supplemented with 0.3% bovine serum albumin (BSA), MEM vitamins, MEM amino acids, L-glutamine and antibiotics/antimycotic (0.3% BSA-MEM), and 0.5 µg/mL TPCK-treated trypsin. The remaining cell lines were infected at an MOI of 0.001 in MEM supplemented with 5% FBS, L-glutamine and antibiotics/antimycotic. All cells were infected in parallel with A/cattle/Texas/56,283/2024 (H5N1) and A/whooper swan/Mongolia/244/2005(H5N1), with inocula in a reduced volume of 0.25 mL per well. After one hour incubation with gentle rocking every 15 min for adsorption, the media were topped up to a final volume of 1.1 mL per well. Aliquots of supernatant were harvested at 24, 48 and 72 HPI for virus titration.

In vivo infections

Eight-week-old BALB/c and 16-week-old C57BL/6 (Jackson Laboratories) mice were anesthetized with isoflurane prior to inoculation by either intranasal administration (virus dilution in 0.3% BSA-MEM, inoculum volume of 60 µl) or oral gavage (virus dilution in grade A raw cow milk, inoculum volume of 100 µl) and, thereafter, monitored at least daily for morbidity (body weight loss, clinical signs of disease) and mortality. Illness severity in infected mice was scored using a standardized 1–4 grading system, as follows: 1, healthy; 2, ruffled fur, lethargic; 3, ruffled fur, lethargic, hunched posture, orbital tightening, labored breathing/dyspnea, and/or more than 15% weight loss; 4, reluctance to move when stimulated or at least 25% weight loss. Score 4 was considered as the humane endpoint, and animals reaching score 4 were immediately euthanized. Euthanasia was performed by asphyxiation with carbon dioxide followed by cervical dislocation.

Mouse median lethal dose (MLD50)

For MLD_{50} determination, eight-week-old BALB/c mice were anesthetized with isoflurane and intranasally inoculated with 10^{-1}, 10^{0}, 10^{1}, 10^{2} or 10^{3} $TCID_{50}$ of A/cattle/Texas/56283/2024 (H5N1) or 10^{1}, 10^{2}, 10^{3}, 10^{4} or 10^{5} $TCID_{50}$ of A/whooper swan/Mongolia/244/2005(H5N1) in 60 µl of 0.3% BSA-MEM, after which mice were monitored at least daily for death or humane endpoint. MLD_{50} was then calculated by the Reed and Muench method[46].

Tissue tropism in mice

Eight-week-old BALB/c mice were anesthetized with isoflurane and intranasally inoculated with 10 $TCID_{50}$ of A/cattle/Texas/56283/2024 (H5N1) or 750 $TCID_{50}$ of. A/whooper swan/Mongolia/244/2005 (H5N1). On days 2, 4, 6 and 8 post-infection, groups of three mice were euthanized and their brains and lungs were harvested and samples were formalin-fixed for histopathological examination or frozen at -80 °C until further processing. Mouse tissues were prepared for virus titration as follows: organ samples were mixed with 1 mL of 0.3% BSA-MEM, homogenized with a TissueLyser (Qiagen) for two cycles of 30 s at 30 Hz with a 1-minute interval, followed by centrifugation at 3,200 × *g* for 10 min at 4 °C. The clarified supernatants were then immediately subjected to virus titration as described below.

Histopathological examination and immunohistochemistry (IHC)

Lungs and brain hemispheres were fixed with 10% neutral-buffered formalin for 72 hours and subsequently sent to the UTMB Histopathology Core for 5 µm paraffin-embedded sections preparation and hematoxylin & eosin (H&E) staining. IHC staining and analysis were performed as previously described, with modifications[47]. In brief, a standard IHC sequential incubation staining protocol was followed to detect the influenza A Matrix 1 protein using a rabbit polyclonal anti-M1 antibody (40010-RP01, Sino Biological, 1:5,000 dilution), followed by peroxidase-conjugated secondary antibody and 3,3'-Diaminobenzidine (DAB) substrate kit (MP-7802, Vector Laboratories). Slides were counterstained with hematoxylin (MHS16-500ML, Sigma-Aldrich) and antigen expression was examined under 10X and 40X magnifications using an Olympus IX71 microscope.

Virus titrations

For determination of median tissue culture infectious dose ($TCID_{50}$), MDCK cells grown in 96-well plates were washed with PBS and inoculated with 10-fold serially diluted samples of supernatants or cell lysates, with four replicates per dilution. Cell monolayers were examined at 3 days post-infection for the development of cytopathic effect (CPE). The $TCID_{50}$ titer was then calculated by the Reed and Muench method[46].

RNA extraction and quantitative RT-PCR

Lungs and brains were homogenized in 1 mL of Trizol reagent (Invitrogen) using TissueLyser (Qiagen), and tissue RNA was extracted using Direct-zol RNA miniprep kits (Zymo research) according to the manufacturer's instructions. Total RNA was then applied to DNA removal process using the Turbo DNA-free kit (Invitrogen), followed by cDNA synthesis using the iScript cDNA synthesis kit (Biorad). Real time PCR reaction was performed using CFX96 real time system (Biorad) and iQ SYBR green supermix (Biorad). All samples were run in duplicate using the following conditions: 95°C for 3 minutes then 45 cycles of 95°C for 5 seconds and 60°C for 30 seconds. The level of expression was then normalized with 18s rRNA and calculated using the 2-ΔΔCt method. Below are primer sets used for this study: mice 18s rRNA (F: 5'-AGTCCCTGCCCTTTGTACACA, R: 5'-CGATCCGAGGGCCTCACTA), mice TNFα (F: 5'- GCCTCTTCTCATTCCTGCTTG, R: 5'- CTGATGAGA GGGAGGCCATT), mice IL-6 (F: 5'- TGAACAACGATGATGCACTTG, R: 5'- CTGAAGGACTCTGGCTTTG TC), mice IFNα (F: 5'- TGCCCAGCAGATCAAGAAGG, R: 5'- TCAGGGGAAATTCCTGCACC), mice IFNβ (F: 5'- GTACAACAGCTACGCCTGGA, R: 5'- GAGTCCGCCTCTGATGCTTA).

Statistical analysis

Unless otherwise stated, comparisons were performed using two-tailed Student's *t*-test. Statistical significance was set at $p < 0.05$ or $p < 0.01$ as indicated in the figure legends.

Data availability

The datasets used and/or analyzed during the current study available from the corresponding author on reasonable request.

Received: 27 December 2024; Accepted: 7 March 2025
Published online: 14 March 2025

References

1. Yamaji, R. et al. Pandemic potential of highly pathogenic avian influenza clade 2.3.4.4 A(H5) viruses. *Rev. Med. Virol.* 30, e; (2099). https://doi.org/10.1002/rmv.2099 (2020).
2. Agüero, M. et al. Highly pathogenic avian influenza A(H5N1) virus infection in farmed Minks, Spain, October 2022. *Euro. Surveill.* **28**, 2300001. https://doi.org/10.2807/1560-7917.ES.2023.28.3.2300001 (2023).
3. Uhart, M. M. et al. Epidemiological data of an influenza A/H5N1 outbreak in elephant seals in Argentina indicates mammal-to-mammal transmission. *Nat. Commun.* **15**, 9516. https://doi.org/10.1038/s41467-024-53766-5 (2024).
4. Peacock, T. et al. The global H5N1 influenza panzootic in mammals. *Nature* https://doi.org/10.1038/s41586-024-08054-z (2024). https://doi.org/10.1038/s41586-024-08054-z Advance online publication.
5. Burrough, E. R. et al. Highly pathogenic avian influenza A(H5N1) clade 2.3.4.4b virus infection in domestic dairy cattle and cats, united States, 2024. *Emerg. Infect. Dis.* **30**, 1335–1343. https://doi.org/10.3201/eid3007.240508 (2024).

6. Oguzie, J. U. et al. Avian influenza A(H5N1) virus among dairy cattle, Texas, USA. *Emerg. Infect. Dis.* **30**, 1425–1429. https://doi.org/10.3201/eid3007.240717 (2024).
7. Mitchell, C. A., Walker, R. V. & Bannister, G. L. Persistence of neutralizing antibody in milk and blood of cows and goats following the instillation of virus into the mammary gland. *Can. J. Comp. Med. Vet. Sci.* **18**, 426–430 (1954).
8. Caserta, L. C. et al. Spillover of highly pathogenic avian influenza H5N1 virus to dairy cattle. *Nature* **634**, 669–676. https://doi.org/10.1038/s41586-024-07849-4 (2024).
9. Nguyen, T. Q. et al. Emergence and interstate spread of highly pathogenic avian influenza A (H5N1) in dairy cattle. *BioRxiv*, 05.01.591751; (2024). https://doi.org/10.1101/2024.05.01.591751 (2024).
10. Animal and Plant Health Inspection Service (APHIS). U. S. Department of Agriculture. HPAI Confirmed Cases in Livestock. (2024). https://www.aphis.usda.gov/livestock-poultry-disease/avian/avian-influenza/hpai-detections/hpai-confirmed-cases-livestock
11. Centers for Disease Control and Prevention (CDC). H5 Bird Flu: Current Situation. (2024). https://www.cdc.gov/bird-flu/situation-summary/index.html
12. Tscherne, D. M. & García-Sastre, A. Virulence determinants of pandemic influenza viruses. *J. Clin. Invest.* **121**, 6–13. https://doi.org/10.1172/JCI44947 (2011).
13. Govorkova, E. A. et al. Susceptibility of highly pathogenic H5N1 influenza viruses to the neuraminidase inhibitor oseltamivir differs in vitro and in a mouse model. *Antimicrob. Agents Chemother.* **53**, 3088–3096. https://doi.org/10.1128/AAC.01667-08 (2009).
14. Lipatov, A. S., Kwon, Y. K., Pantin-Jackwood, M. J. & Swayne, D. E. Pathogenesis of H5N1 influenza virus infections in mice and ferret models differs according to respiratory tract or digestive system exposure. *J. Infect. Dis.* **199**, 717–725. https://doi.org/10.1086/596740 (2009).
15. Giles, B. M. & Ross, T. M. A computationally optimized broadly reactive antigen (COBRA) based H5N1 VLP vaccine elicits broadly reactive antibodies in mice and ferrets. *Vaccine* **29**, 3043–3054. https://doi.org/10.1016/j.vaccine.2011.01.100 (2011).
16. Giles, B. M. et al. A computationally optimized hemagglutinin virus-like particle vaccine elicits broadly reactive antibodies that protect nonhuman primates from H5N1 infection. *J. Infect. Dis.* **205**, 1562–1570. https://doi.org/10.1093/infdis/jis232 (2012).
17. Eisfeld, A. J. et al. Pathogenicity and transmissibility of bovine H5N1 influenza virus. *Nature* **633**, 426–432. https://doi.org/10.1038/s41586-024-07766-6 (2024).
18. Tipih, T. et al. Recent Bovine HPAI H5N1 Isolate is Highly Virulent for Mice, Rapidly Causing Acute Pulmonary and Neurologic Disease. *BioRXiv*, 08.19.608652; (2024). https://doi.org/10.1101/2024.08.19.608652 (2024).
19. Mogensen, T. H. & Paludan, S. R. Molecular pathways in virus-induced cytokine production. *Microbiol. Mol. Biol. Rev.* **65**, 131–150. https://doi.org/10.1128/MMBR.65.1.131-150.2001 (2001).
20. Liu, Q., Zhou, Y. H. & Yang, Z. Q. The cytokine storm of severe influenza and development of Immunomodulatory therapy. *Cell Mol. Immunol.* **13** (1), 3–10. https://doi.org/10.1038/cmi.2015.74 (2016).
21. Guo, X. J. & Thomas, P. G. New fronts emerge in the influenza cytokine storm. *Semin Immunopathol.* **39**, 541–550. https://doi.org/10.1007/s00281-017-0636-y (2017).
22. Gu, Y. et al. The mechanism behind influenza virus cytokine storm. *Viruses* **13**, 1362. https://doi.org/10.3390/v13071362 (2021).
23. Ryabkova, V. A., Churilov, L. P. & Shoenfeld, Y. Influenza infection, SARS, MERS and COVID-19: cytokine storm - the common denominator and the lessons to be learned. *Clin. Immunol.* **223**, 108652. https://doi.org/10.1016/j.clim.2020.108652 (2021).
24. Marc, D. Influenza virus non-structural protein NS1: interferon antagonism and beyond. *J. Gen. Virol.* **95**, 2594–2611. https://doi.org/10.1099/vir.0.069542-0 (2014).
25. Varga, Z. T., Grant, A., Manicassamy, B. & Palese, P. Influenza virus protein PB1-F2 inhibits the induction of type I interferon by binding to MAVS and decreasing mitochondrial membrane potential. *J. Virol.* **86**, 8359–8366. https://doi.org/10.1128/JVI.01122-12 (2012).
26. Xia, C. et al. Hemagglutinin of influenza A virus antagonizes type I interferon (IFN) responses by inducing degradation of type I IFN receptor 1. *J. Virol.* **90**, 2403–2417. https://doi.org/10.1128/JVI.02749-15 (2015).
27. Yang, H. et al. The influenza virus PB2 protein evades antiviral innate immunity by inhibiting JAK1/STAT signalling. *Nat. Commun.* **13**, 6288. https://doi.org/10.1038/s41467-022-33909-2 (2022).
28. Goubau, D., Deddouche, S., Reis & Sousa, C. Cytosolic sensing of viruses. *Immunity* **38**, 855–869. https://doi.org/10.1016/j.immuni.2013.05.007 (2013).
29. Takaoka, A. & Yamada, T. Regulation of signaling mediated by nucleic acid sensors for innate interferon-mediated responses during viral infection. *Int. Immunol.* **31**, 477–488. https://doi.org/10.1093/intimm/dxz034 (2019).
30. Katze, M. G., He, Y. & Gale, M. Jr. Viruses and interferon: a fight for supremacy. *Nat. Rev. Immunol.* **2**, 675–687. https://doi.org/10.1038/nri888 (2002).
31. Sengupta, P. & Chattopadhyay, S. Interferons in viral infections. *Viruses* **16**, 451. https://doi.org/10.3390/v16030451 (2024).
32. United States Department of Agriculture. USDA, HHS Announce New Actions to Reduce Impact and Spread of H5N1. Fact Sheet Release No.:0082.24. (2024). https://www.usda.gov/article/usda-hhs-announce-new-actions-reduce-impact-and-spread-h5n1
33. Gu, C. et al. A human isolate of bovine H5N1 is transmissible and lethal in animal models. *Nature* https://doi.org/10.1038/s41586-024-08254-7 (2024). Epub ahead of print.
34. Guan, L. et al. Cow's milk containing avian influenza A(H5N1) Virus - Heat inactivation and infectivity in mice. *N Engl. J. Med.* **391**, 87–90. https://doi.org/10.1056/NEJMc2405495 (2024).
35. Government of Canada. Statement from the Public Health Agency of Canada: Update on Avian Influenza and Risk to Canadians. (2024). https://www.canada.ca/en/public-health/news/2024/11/update-on-avian-influenza-and-risk-to-canadians.html
36. Centers for Disease Control and Prevention (CDC). CDC confirms first severe case of H5N1 bird flu in the united States. *CDC Newsroom* (2024). https://www.cdc.gov/media/releases/2024/m1218-h5n1-flu.html
37. Basler, C. F. et al. The Ebola virus VP35 protein functions as a type I IFN antagonist. *Proc. Natl. Acad. Sci.* **97**, 12289–12294. https://doi.org/10.1073/pnas.220398297 (2000).
38. Cárdenas, W. B. et al. Ebola virus VP35 protein binds double-stranded RNA and inhibits alpha/beta interferon production induced by RIG-I signaling. *J. Virol.* **80**, 5168–5178. https://doi.org/10.1128/JVI.02199-05 (2006).
39. Basler, C. F. & Amarasinghe, G. K. Evasion of interferon responses by Ebola and Marburg viruses. *J. Interferon Cytokine Res.* **29**, 511–520. https://doi.org/10.1089/jir.2009.0076 (2009).
40. Kühl, A. & Pöhlmann, S. How Ebola virus counters the interferon system. *Zoonoses Public. Health.* **59**, 116–131. https://doi.org/10.1111/j.1863-2378.2012.01454.x (2012).
41. Villinger, F. et al. Markedly elevated levels of interferon (IFN)-gamma, IFN-alpha, Interleukin (IL)-2, IL-10, and tumor necrosis factor-alpha associated with fatal Ebola virus infection. *J. Infec Dis.* **179**, S188–S191. https://doi.org/10.1086/514283 (1999).
42. Hensley, L. E., Young, H. A., Jahrling, P. B. & Geisbert, T. W. Proinflammatory response during Ebola virus infection of primate models: possible involvement of the tumor necrosis factor receptor superfamily. *Immunol. Lett.* **80**, 169–179. https://doi.org/10.1016/s0165-2478(01)00327-3 (2002).
43. Caballero, I. S. et al. In vivo Ebola virus infection leads to a strong innate response in Circulating immune cells. *BMC Genom.* **17**, 707. https://doi.org/10.1186/s12864-016-3060-0 (2016).
44. Zhu, W. Y., Tao, X. Y., Lyu, X. J., Yu, P. C. & Lu, Z. Z. Enhancement of virus replication in an influenza A virus NS1-expresssing 293 cell line. *Biomed. Environ. Sci.* **29**, 224–228 (2016).

45. Eisfeld, A. J., Neumann, G. & Kawaoka, Y. Influenza A virus isolation, culture and identification. *Nat. Protoc.* **9**, 2663–2681. https://doi.org/10.1038/nprot.2014.180 (2014).
46. Reed, L. J. & Muench, H. A simple method of estimating Fifty per cent endpoints. *Am. J. Epidemiol.* **27**, 493–497 (1938).
47. Tseng, C. T. et al. Severe acute respiratory syndrome coronavirus infection of mice Transgenic for the human Angiotensin-converting enzyme 2 virus receptor. *J. Virol.* **81**, 1162–1173. https://doi.org/10.1128/JVI.01702-06 (2007).

Acknowledgements
We thank Dr. Junki Maruyama for kindly providing us with the MDBK cell line, and the World Reference Center for Emerging Viruses and Arboviruses (WRCEVA), University of Texas Medical Branch, for providing the cattle H5N1 virus used in this study. The Calu-3 cell lines overexpressing GFP, RIG-I and MDA5 used in this study were previously generated in our laboratory by Shuetsu Fukushi.

Author contributions
C.P.O.: conceptualization, performed experiments, analyzed data, wrote the main manuscript text. P.H.: conceptualization, performed experiments, analyzed data, prepared figures, wrote manuscript. P.B.: analyzed histopathology, prepared Fig. 4, wrote manuscript. G.C.G.: provided materials, revised manuscript. C.K.T.: conceptualization, supervision, revised manuscript. C.P.O. and P.H. contributed equally to this work. All authors reviewed the manuscript.

Declarations

Competing interests
The authors declare no competing interests.

Additional information
Supplementary Information The online version contains supplementary material available at https://doi.org/10.1038/s41598-025-93493-5.

Correspondence and requests for materials should be addressed to C.P.O., P.H. or C.-T.K.T.